AGU PUBLICATIONS

Geophysical Research Letters

RESEARCH LETTER
10.1002/2013GL058956

Key Points:
- Warm waters intrusion from the Mackenzie River discharge impacts sea ice melt
- Strong Beaufort Gyre fragmented sea ice to precondition and enhance melting
- Arctic rivers constitute the starkest contrast to Antarctic without such river

Supporting Information:
- Readme
- Table S1
- Table S2
- Figure S1
- Figure S2
- Figure S3
- Figure S4
- Figure S5

Correspondence to:
S. V. Nghiem,
Son.V.Nghiem@jpl.nasa.gov

Citation:
Nghiem, S. V., D. K. Hall, I. G. Rigor, P. Li, and G. Neumann (2014), Effects of Mackenzie River discharge and bathymetry on sea ice in the Beaufort Sea, *Geophys. Res. Lett.*, *41*, doi:10.1002/2013GL058956.

Received 5 DEC 2013
Accepted 17 JAN 2014
Accepted article online 20 JAN 2014

Effects of Mackenzie River discharge and bathymetry on sea ice in the Beaufort Sea

S. V. Nghiem[1], D. K. Hall[2], I. G. Rigor[3], P. Li[1], and G. Neumann[1]

[1]Jet Propulsion Laboratory, California Institute of Technology, Pasadena, California, USA, [2]NASA Goddard Space Flight Center, Greenbelt, Maryland, USA, [3]University of Washington, Seattle, Washington, USA

Abstract Mackenzie River discharge and bathymetry effects on sea ice in the Beaufort Sea are examined in 2012 when Arctic sea ice extent hit a record low. Satellite-derived sea surface temperature revealed warmer waters closer to river mouths. By 5 July 2012, Mackenzie warm waters occupied most of an open water area about 316,000 km^2. Surface temperature in a common open water area increased by 6.5°C between 14 June and 5 July 2012, before and after the river waters broke through a recurrent landfast ice barrier formed over the shallow seafloor offshore the Mackenzie Delta. In 2012, melting by warm river waters was especially effective when the strong Beaufort Gyre fragmented sea ice into unconsolidated floes. The Mackenzie and other large rivers can transport an enormous amount of heat across immense continental watersheds into the Arctic Ocean, constituting a stark contrast to the Antarctic that has no such rivers to affect sea ice.

1. Introduction

The total extent of Arctic sea ice hit a record low in the summer of 2012 within the era of satellite observations spanning over three decades [*Perovich et al*., 2013]. A number of explanations have been suggested, including vulnerability to the great Arctic cyclone of August 2012 [*Simmonds and Rudeva*, 2012], sea ice preconditioning from winter through early summer [*Devasthale et al*., 2013], combined effects of the storm and preconditioning [*Parkinson and Comiso*, 2013], and upward ocean heat transport from enhanced ocean mixing [*Zhang et al*., 2013]. Here we consider a different factor—warm waters from river discharge—in melting sea ice in 2012. In particular, we show that the warm waters of the Mackenzie River discharged into the Beaufort Sea, where sea ice had been fragmented into small floes by strong winds on the Beaufort Gyre (BG) in early July 2012 before the August storm occurred. Furthermore, we examine how the seafloor controls the recurrent pattern of sea ice and the release of the Mackenzie discharge into the Beaufort Sea. We also contrast the Arctic Ocean situation with that of the Southern Ocean.

2. Sea Ice in the Beaufort Sea Study Domain in 2012 Compared to Changes in 1979–2011

Sea ice has reduced severely in the Beaufort Sea [*Ogi and Rigor*, 2013; *Perovich et al*., 2007]. The current sea ice cover consists of thinner, younger, and weaker ice that facilitates lead formation and influences halogen chemical processes [*Nghiem et al*., 2013] and mercury deposition [*Steffen et al*., 2013]. Sea ice reduction in the Beaufort Sea may also shorten the snow season and adversely impact the habitat of ringed seals [*Kelly et al*., 2007].

In this study, the Beaufort Sea domain of interest is bounded by longitudes 123°W–147°W, latitude 74°N in the north, and the coastline along the south side. Within this region, satellite active microwave scatterometer (AMS) and passive microwave radiometer (PMR) data are used to observe the change in sea ice extent (SIE) in early summer over the past three decades. A difficulty in summer observations of sea ice is that surface melt can impact PMR signatures of sea ice, causing large uncertainties in the measurement of SIE.

To alleviate this problem, an AMS algorithm was developed to determine SIE, primarily using a quadruplet combination of relative AMS values rather than the absolute magnitudes of the signature and thus improving SIE accuracy [*Nghiem et al*., 2005]. QuikSCAT data in 2000–2009 are processed with the AMS algorithm to determine SIE average over 1–7 July in each year. Then the AMS results are applied to select an optimal value of PMR sea ice concentration (SIC), available at the *National Snow and Ice Data Center* [2013] in Boulder,

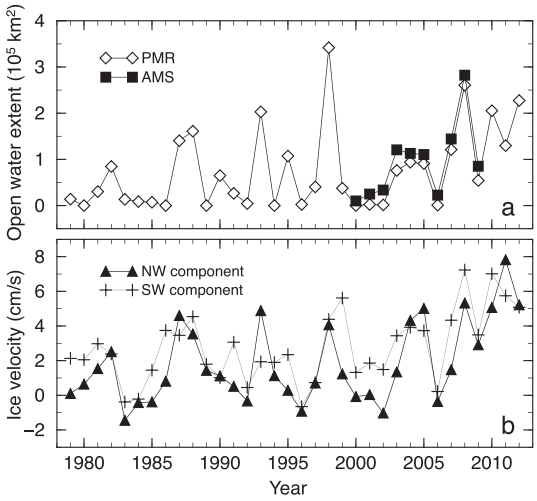

Figure 1. (top) For open water extent within the study domain in the Beaufort Sea observed by satellite PMR data (1979–2012) and AMS data (2000–2009) averaged over 1–7 July and (bottom) for ice velocity in the NW and SW orthogonal components at the center of the study domain averaged over May–June in each year. A positive velocity value indicates ice moving toward the NW or the SW direction.

Colorado, to obtain a long-term time series of SIE in the Beaufort Sea study domain consistently between both AMS and PMR data sets. SIE results in 1979–2012 for SIC above the optimal threshold of 0.1, which best matches AMS and PMR SIE in the common decade of 2000–2009, are used to calculate open water extent. Figure 1a shows a large extent of open water in 2012, a larger open water extent in 2008, and the record high extent in 1998. *Rawlins et al*. [2009] reported a record discharge from the Mackenzie River in May 1998, and *Perovich et al*. [2011] showed significant underside ice melt resulting from solar heat input in 2008. Thus, we will examine the role of warm waters from river discharge in accelerating sea ice melt, which leads to earlier and more extensive open water having a lower albedo and allowing more solar heat absorption [*Perovich et al*., 2007].

The change in SIE is affected by dynamic and thermodynamic conditions of sea ice. In the Beaufort Sea, sea ice characteristics can change depending on the variable strength of BG activities driven by atmospheric and oceanic forcing. To quantify the BG strength, average values of sea ice velocity in the NW and SW orthogonal components at the center of the study domain in May–June are calculated from buoy data provided by the International Arctic Buoy Programme [*Rigor*, 2005]. The sea ice velocity (Figure 1b) is correlated with the open water extent in 1979–2012 with a correlation coefficient of 0.77 for the NW and 0.68 for the SW component. When the data are detrended to assess the correlation of the interannual variability, the correlation coefficients remain relatively high at 0.72 and 0.60 for the NW and SW components of the sea ice velocity, respectively. The overall ice velocity was mostly toward the west, moving away from the Canadian Arctic archipelago toward the Canada Basin unrestricted by land, facilitating sea ice divergence. Thus, strong BG activities in May–June can fragment sea ice and precondition it for enhanced melting from the subsequent intrusion of the Mackenzie warm waters in early July 2012.

3. Bathymetry Effects

To examine further details in the case of the large open water extent in July 2012, Moderate Resolution Imaging Spectroradiometer (MODIS) images are used to observe sea ice change in this region. Figure 2 is an overlay of two images acquired on 14 June 2012 and 17 May 2013 by the Terra MODIS. Each image is a composite of bands 1, 2, and 7 (620–670, 841–876, and 2105–2155 nm wavelengths) with a pixel size of 250 m in the MODIS Rapid Response subset generated for near-real-time support of the Bromine, Ozone, and Mercury Experiment [*Nghiem et al*., 2013]. The sea ice pattern on 14 June 2012 (light blue) reveals a band of landfast sea ice off the coast of the Mackenzie River Delta. The edge of this landfast sea ice traces consistently well along a lead (black elongated feature) opened up in the sea ice cover (dark cyan) on 17 May 2013.

The recurrence of the sea ice fracture suggests a control exerted by the shallow bathymetry shaping sea ice patterns in this littoral zone. In fact, the lead in 2013 and the landfast ice edge in 2012 are both found to conform the best to the 25 m isobath by a bathymetry conformity analysis [*Nghiem et al*., 2012] with data from the International Bathymetric Chart of the Arctic Ocean (IBCAO) [*Jakobsson et al*., 2008, 2012]. The ice edges conform well to the 25 m isobath (Figure S1 in the supporting information), regardless how close (i.e., steep slope) or how far apart (i.e., gradual slope) the other isobaths are separated from the 25 m isobath. These results show that sea ice patterns are controlled by bathymetric depth and are independent of seafloor slope (see Figure S1 and Table S1).

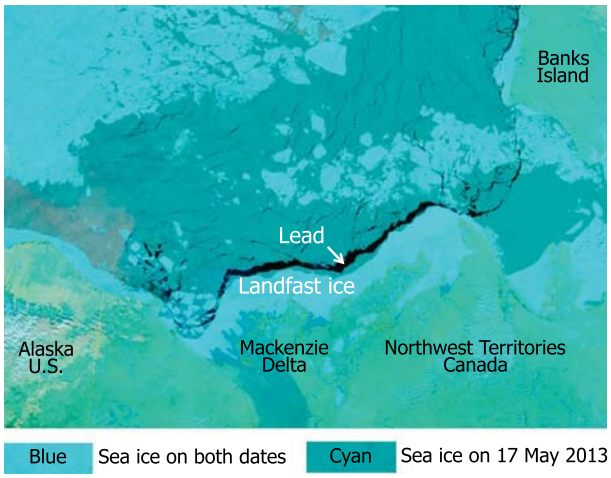

Figure 2. Sea ice in the Beaufort Sea observed by a combination of bands 1, 2, and 7 from data acquired by MODIS aboard the Terra satellite. The 17 May 2013 MODIS image is translucently overlain over the 14 June 2012 MODIS image. Light blue is for sea ice existing on both dates, cyan for sea ice only on 17 May 2013, and black for no sea ice on either date. The landfast sea ice in 2012 is observed as the light blue band in the littoral zone along the coast of the Mackenzie Basin, and the large long lead in 2013 is seen as the long black fracture tracing along the edge of the 2012 landfast ice.

Constrained by bathymetric effects, the stability of the landfast ice extent has been observed over the past several decades. From Advanced Very High Resolution Radiometer and Landsat data in 1986, *Dean et al*. [1994] saw a similar band of landfast sea ice off the Mackenzie River Delta. Using Radarsat imagery acquired in 1996–2004 across the eastern Chukchi Sea to the western Beaufort Sea, *Mahoney et al*. [2007] found broad stable extensions of landfast sea ice, which did not show any significant difference from the 1970s. The recurrence of the Mackenzie landfast ice feature, which determines the timing of the warm river discharge breakthrough and thus the timing of sea ice melt acceleration, can help in sea ice forecasting for operational applications.

It is noted that the landfast sea ice edge in 2012 and the lead in 2013 trace well along the 25 m isobath from IBCAO version 2, except over the local seafloor features marked inside the red ellipse (Figure S1). Those features were erroneous artifacts in IBCAO version 2, which was corrected by new survey data in IBCAO version 3. The new 25 m isobath from IBCAO version 3 matches all along the 2012 ice edge and the 2013 lead very well (Figure S1). These results suggest that recurrent sea ice patterns, once detected, can be useful for planning future bathymetry survey missions.

The pattern of bathymetric isobaths can be a good indicator for landfast sea ice extent in the Beaufort Sea [*Mahoney et al*., 2007], and sea ice can conform to bathymetry recurrently in different years (Figure S1). However, the ice edge may not necessarily have to follow exactly along the same isobath all the time due to anomalous atmospheric (winds) or oceanic (currents) forcing that may become so strong to overwhelm bathymetry effects.

4. Warm Waters of the Mackenzie River

To investigate the distribution pattern of surface waters in the Beaufort Sea, two different algorithms are used to measure surface temperature from MODIS. The first is the ice surface temperature (IST) algorithm (called AG1 hereon), which was originally developed with a split-window technique to map snow or ice surface temperature at a resolution of 1 km [*Hall et al*., 2004]. This is the standard MODIS IST product, MOD29 [*Riggs et al*., 2006], implemented at the Goddard Space Flight Center and available through National Snow and Ice Data Center with approximately 24 h latency. Here AG1 is applied to measure temperature of the ocean water surface or sea surface temperature (SST).

The second algorithm (AG2) produces daily global 1 km SST maps using Level-2 preprocessed data products from the Global High-Resolution SST Pilot Project and in situ ship and buoy measurements from the Global Ocean Data Assimilation Experiment server. A multiscale two-dimensional variational blending algorithm was used to combine all input data products and output SST [*Chao et al*., 2009]. The SST data are available at the Jet Propulsion Laboratory (JPL) Physical Oceanography Distributed Active Archive Center with approximately 24 h latency [*JPL OurOcean Project*, 2013].

To observe the change caused by warm waters from the Mackenzie discharge, open water surface temperature (OWST) in the Beaufort Sea study domain is compared before and after the landfast sea ice barrier was breached to release the waters from the Mackenzie River into the Beaufort Sea. On 14 June 2012, while the open water area (Figure 3a) was estimated at about 210,600 km^2, Mackenzie waters were still obstructed by the landfast sea ice barrier. This is evident in Figure 2 showing the band of landfast sea ice (light blue) across

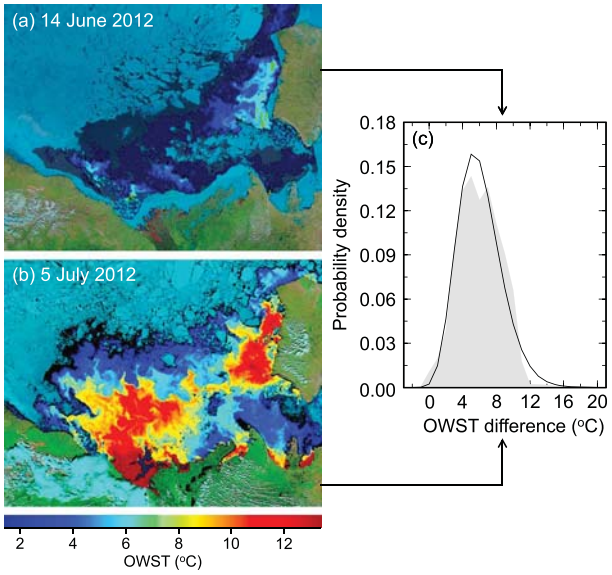

Figure 3. Open water surface temperature (OWST) in °C, measured by MODIS AG1 on 14 June 2012 (a) before the Mackenzie River water broke through the landfast sea ice barrier, and on 5 July 2012 (b) after warm waters from the Mackenzie discharged into the Beaufort Sea. Sea ice is indicated by the steel blue color on the sea surface. (c) For the measured and calculated histograms of the temperature difference in °C between the two cases in Figures 3a and 3b. The temperature difference is calculated over each pixel that is open water in both cases.

the mouths of streams where the warm waters intruded into the ice barrier and created several fingers of water overflows that had not yet reached to the landfast ice edge. See Figure S2 for the close-up detail of the water fingers; similar overflow patterns were observed in 1986 [*Dean et al.*, 1994]. Clear sky conditions on 14 June allow the use of MODIS satellite data to estimate the Beaufort Sea OWST. As seen in Figure 3a, OWST was low while the landfast ice hindered the river discharge. A pattern of warm waters was observed to the west of Banks Island, possibly from the inland water runoff.

OWST on 5 July 2012 (Figure 3b) reveals the extrusion of warm waters in the Beaufort Sea when the landfast sea ice had disappeared and the stream mouths were fully opened for water discharge from the Mackenzie River. By that time, the area of open water observed by MODIS in this region was 316,000 km^2, about the size of the country of Italy or Poland. The warmest waters were observed near the coast of the Mackenzie Delta, e.g., 13°C at 147 km, 10°C at 287 km, 8°C at 350 km, and 2°C as far as 456 km from the Mackenzie River mouth. As the warm river waters extended farther out into the Beaufort Sea, OWST became lower and mixed with cooler waters in a complex swirling pattern (Figure 3b). The warm waters in the west of Banks Island also became more extensive and started to connect to the Mackenzie warm waters mass. OWST was lower toward the sea ice edge in the Canada Basin where the water temperature still maintained above freezing temperatures. OWST patterns obtained from AG1 and AG2 are closely consistent and thus only the AG1 temperature is shown in Figure 3. In fact, a comparison of OWST from AG1 and AG2 in this case shows that the mean difference is only 0.2°C, although AG1 OWST can be lower by 0.75°C at the minimum and higher by 1.3°C at the maximum of the temperature range compared to AG2 values. Patterns of OWST in 1998 and 2008 reveal a similar spatial structure with warmer waters closer to the river mouth (see Figures S3 and S4).

To obtain a quantitative assessment of the increase in OWST after the intrusion of the warm river waters into the Beaufort Sea, each pixel that was observed as open water in both cases on 14 June and 5 July was selected to calculate the temperature difference. The histogram of this temperature difference is presented in Figure 3c. The result shows a mean increase in OWST of 6.5°C between the two cases before and after the Mackenzie warm waters intrusion. The statistics of the OWST difference is similar to the characteristics of the gamma distribution, which is traditionally used to model waiting times until a termination event, such as death in life testing [*Hogg et al.*, 2012] or sea ice extinction in this case. Quantitatively, the probability density function of the OWST difference is determined by the gamma distribution

$$f_p(\Delta T) = (\Delta T + T_c)^{k-1} \exp[-(\Delta T + T_c)/\theta] / [\theta^k \Gamma(k)] \quad (1)$$

where Γ is the gamma function, ΔT is the OWST difference, $T_c = 3.0$°C, $k = 12.2206$, and $\theta = 0.740481$, which are determined numerically by requiring that both measured and calculated values of the probability density have the same mean, variance, and skewness (Figure 3c).

5. Summary and Discussions

In summary, two different algorithms were used with MODIS satellite data to observe the intrusion of warm waters from the Mackenzie River discharge into the Beaufort Sea. Results from both algorithms agreed well

and consistently revealed the large increase in OWST after the warm river waters broke through the landfast sea ice barrier. The water temperature increase significantly contributed to melting sea ice that had been fragmented into unconsolidated ice floes by strong winds on the Beaufort Gyre.

In the study domain, the open water extent increased by 50% in 3 weeks from14 June to 5 July 2012, a month before the great Arctic cyclone occurred in August 2012. In this process, the shallow coastal bathymetry can exert control on the formation of the landfast sea ice barrier that obstructs the river discharge until its removal. Early model results indicated that the coastal sea ice under the riverine influence could be removed 1 to 2 weeks in advance of areas without significant river discharge [*Searcy et al*., 1996]. At larger scales, bathymetry effects on sea ice formation in the Beaufort Sea were also reported [*Carmack and Chapman*, 2003; *Nghiem et al*., 2012]. Since bathymetry does not change significantly over long geological time scales, it provides a systematic memory allowing the recurrent formation of the landfast sea ice barrier in different years. Such a stable geological memory from the bathymetry should be included to improve the predictability in sea ice models [*Nghiem et al*., 2012].

The Mackenzie discharge typically peaks in June and remains high in July [*Woo and Thorne*, 2003]. For a peak flow of 33,300 m^3/s [*Environment Canada*, 2013], the volume of the total discharge over the 3 week period is equivalent to a layer thickness of 0.19 m of warm waters across the entire open water area of 316,000 km^2 on 5 July 2012. Note that this is only a uniform equivalence representation of the warm waters mass, while actual distribution of the waters can have complex mixing patterns (Figure 3). The extensive waters intrusion from the Mackenzie River was also identifiable by terrestrial dissolved organic matter traced by an optical proxy from MODIS spectral data [*Fichot et al*., 2013].

The Mackenzie River has an enormous watershed of 1.8 million km^2 with the southern extent reaching to 52.2°N (see Figure S5 and Table S2). This watershed is primarily within the continental climate regime, and the heat can be intense in summer when the maximum temperature may reach 32°C around latitude 53°N (e.g., Edmonton, Alberta, Canada). Fresh and warm Mackenzie waters reside in the surface layer (Figure 3) with the attendant high thermal capacity thus contributing excessive heat to melt sea ice, most effectively when the sea ice cover has been fragmented by the strong BG. This was the case in the 1998 melt season when ice velocity was high in the BG (Figure 1), the Mackenzie River had a record discharge [*Rawlins et al*., 2009], and a record high of open water extent was observed in the decadal satellite data (Figure 1).

The Mackenzie River is a highly effective conveyor that transports continental heat into the Beaufort Sea contributing to the overall heat budget for sea ice melting. While Mackenzie discharge had no discernable trend in 1972–1999 [*Woo and Thorne*, 2003], an increasing trend in the mean air temperature was identified in station data in 1948–2007 [*Turner and Gyakum*, 2010], especially over the Mackenzie watershed in western Canada. Even assuming no temperature increase in Mackenzie River waters, the warm discharge can still effectively melt sea ice because Arctic sea ice, especially in the Beaufort Sea, has shifted to a new regime dominated by seasonal sea ice that is younger, thinner, and weaker [*National Academies*, 2012]. Such diminished sea ice becomes easily fragmented into small ice floes that increase the ice interface with warm waters to accelerate the melt process.

In addition to the Mackenzie, there are a number of other large rivers that discharge into the Arctic Ocean. Notable are the Yukon, Ob, Yenisei, Lena, and Kolyma Rivers (see Table S2), each with its immense watershed under a continental climate regime providing massive discharge of warm waters into the Arctic Ocean or a peripheral sea to melt sea ice in spring and summer. Extensive intrusions of river runoff traced by a MODIS optical proxy have been reported [*Fichot et al*., 2013]. A large increase from the Eurasian rivers together with a small decrease from North America resulted in a net discharge increase by 5.6 km^3/yr^2 into the Arctic Ocean during 1964–2000 with a mean annual discharge from the mouths of 72 rivers totaled to over 2.5 trillion m^3 by 2000 [*McClelland et al*., 2006], and the 2011 Arctic Report Card showed similar volume of total annual discharge from large Arctic rivers [*Shiklomanov and Lammers*, 2011]. This massive discharge carries an enormous heating power of 1.0×10^{19} J/yr for each 1°C of the warm river waters above freezing, equivalent to 2.5 gigaton of trinitrotoluene (TNT) per °C per year. As a comparison, Antarctic mass loss was approximately 200 ± 150 Gt/yr by 2006 at a rate of -14.5 ± 2 Gt/yr^2 [*Rignot et al*., 2011]. When projected to 2010, the Antarctic total mass loss amounts only to about 10% of the Arctic total river discharge in the annual mean. This is a stark contrast between the Arctic with drastic sea ice decrease and Antarctic with stable (or somewhat increasing) sea ice since there is no such massive river discharge from the Antarctic continent, primarily

a frozen continent located at high latitudes and high altitudes around the South Pole. However, river discharge is not the only factor leading to the difference between Arctic and Antarctic sea ice. Other factors are bathymetry that guides waters distribution and circulation in the Southern Ocean, and topography on the Antarctic continent that controls the katabatic wind. These stable geological factors contribute to the stability of the Antarctic sea ice cover [*Nghiem*, 2013].

In the summer melt season, warm river waters, for which the temperatures can be higher than 10°C (Figure 3b), contribute directly to melting sea ice. In the fall season around the time of sea ice freezeup, surface waters cool while the halocline stratification insulates the surface from the deeper seawater, allowing more sea ice to grow. At the same time in the fall, rivers also start to freezeup, drastically reducing the river discharge. Thus, to be an effective insulator, the stratification needs to be persistent to maintain the surface layer consisting of a large mass of fresh river waters that already discharged into the Arctic Ocean earlier in the summer. Such maintenance of the stratification requires calm-ocean conditions without significant mixing throughout the summer to fall freezeup. In summer 2012, the violent storm significantly enhanced ocean mixing that transported ocean heat upward and further contributed to sea ice melt [*Zhang et al*., 2013].

While this paper presents surface patterns of the Mackenzie warm waters intrusion into the Beaufort Sea, future hydrograph surveys using ship or buoys to measure temperature and salinity profiles across the Mackenzie discharge domain are necessary to determine the three-dimensional mixing for a rigorous assessment of the total heat content in warm waters available to melt sea ice. In particular, there is a severe lack of river water temperature profile data across river channels or river mouths where warm waters discharge into the Arctic Ocean. Such river temperature data are required to calculate the regional as well as total thermal heating power carried by the river waters to melt sea ice. This is a critical knowledge gap that needs to be addressed by systematic and well-calibrated networks of sensors for long-term river temperature measurement. While in situ data are available at river gauging stations in land, stream flow and river discharge can be measured with multidecadal data sets acquired by multiple satellite sensors [*Brakenridge et al*., 2007] at many river reaches including locations near river mouths for long-term quantitative analyses. Rigorous interdisciplinary studies for all large Arctic rivers are necessary to understand the overall contribution and interactions of the discharged warm waters in melting sea ice. In this respect, it is crucial to monitor river change, including discharge and temperature, with adequate, continuous, and accurate measurements by river gauges, buoy networks, and satellite sensors.

Acknowledgments

The research carried out at the Jet Propulsion Laboratory (JPL), California Institute of Technology, and at NASA Goddard Space Flight Center (GSFC) was supported by the National Aeronautics and Space Administration (NASA) Cryospheric Sciences Program. Rigor is funded by NASA and other contributors to the U.S. Interagency Arctic Buoy Program. We thank Jody Hoon-Starr and Nick DiGirolamo of Science Systems and Applications, Inc. (SSAI), and Lisa Nguyen of JPL for programming help. We thank Michael Dettinger of the U.S. Geological Survey for his help with additional river discharge data.

The Editor thanks John Falkingham and an anonymous reviewer for their assistance in evaluating this paper.

References

Brakenridge, G. R., S. V. Nghiem, E. Anderson, and R. Mic (2007), Orbital microwave measurement of river discharge and ice status, *Water Resour. Res.*, *43*, W04405, doi:10.1029/2006WR005238.

Carmack, E., and D. C. Chapman (2003), Wind-driven shelf/basin exchange on an Arctic shelf: The joint roles of ice cover extent and shelf-break bathymetry, *Geophys. Res. Lett.*, *30*(14), 1778, doi:10.1029/2003GL017526.

Chao, Y., Z. Li, J. D. Farrara, and P. Huang (2009), Blended sea surface temperatures from multiple satellites and in-situ observations for coastal oceans, *J. Atmos. Oceanic Technol.*, *26*, 1415–1426, doi:10.1175/2009JTECHO592.1.

Dean, K. G., W. J. Stringer, K. Ahlnäs, C. Searcy, and T. Weingartner (1994), The influence of river discharge on the thawing of sea ice, Mackenzie River Delta: Albedo and temperature analyses, *Polar Res.*, *13*(1), 83–94.

Devasthale, A., J. Sedlar, T. Koenigk, and E. J. Fetzer (2013), The thermodynamic state of the Arctic atmosphere observed by AIRS: Comparisons during the record minimum sea ice extents of 2007 and 2012, *Atmos. Chem. Phys.*, *13*(15), 7441–7450, doi:10.5194/acp-13-7441-2013.

Environment Canada (2013), Rivers. [Available at http://www.ec.gc.ca/eau-water/default.asp?lang=En&n=45BBB7B8-1, accessed Nov. 2013.]

Fichot, C. G., K. Kaiser, S. B. Hooker, R. M. Amon, M. Babin, S. Bélanger, S. A. Walker, and R. Benner (2013), Pan-Arctic distributions of continental runoff in the Arctic Ocean, *Sci. Rep.*, *3*(1053), 1–6, doi:10.1038/srep01053.

Hall, D. K., J. Key, K. A. Casey, G. A. Riggs, and D. J. Cavalieri (2004), Sea ice surface temperature product from MODIS, *IEEE Trans. Geosci. Remote Sens.*, *42*, 1076–1087.

Hogg, R. V., J. McKean, and A. T. Craig (2012), *Introduction to Mathematical Statistics*, 7th ed., 640 pp., Pearson Publisher, Boston, Mass.

Jakobsson, M., R. Macnab, L. Mayer, R. Anderson, M. Edwards, J. Hatzky, H. W. Schenke, and P. Johnson (2008), An improved bathymetric portrayal of the Arctic Ocean: Implications for ocean modeling and geological, geophysical and oceanographic analyses, *Geophys. Res. Lett.*, *35*, L07602, doi:10.1029/2008GL033520.

Jakobsson, M., et al. (2012), The International Bathymetry Chart of the Arctic Ocean (IBCAO) version 3.0, *Geophys. Res. Lett.*, *39*, L12609, doi:10.1029/2012GL052219.

JPL OurOcean Project (2013), GHRSST Level 4 G1SST Global Foundation Sea Surface Temperature Analysis. [Available at http://podaac.jpl.nasa.gov/dataset/JPL_OUROCEAN-L4UHfnd-GLOB-G1SST, accessed Jan. 2013.]

Kelly, B. P., J. Moran, D. C. Douglas, and S. V. Nghiem (2007), Monitor snow on ice as critical habitat for ringed seals, *Eos Trans. AGU*, *88*(52), Fall Meet. Suppl., Abst. C23B-08.

Mahoney, A., H. Eicken, A. G. Gaylord, and L. Shapiro (2007), Alaska landfast sea ice: Links with bathymetry and atmospheric circulation, *J. Geophys. Res.*, *112*, C02001, doi:10.1029/2006JC003559.

McClelland, J. W., S. J. Déry, B. J. Peterson, R. M. Holmes, and E. F. Wood (2006), A pan-arctic evaluation of changes in river discharge during the latter half of the 20th century, *Geophys. Res. Lett.*, *33*, L06715, doi:10.1029/2006GL025753.

National Academies (2012), *Seasonal to Decadal Predictions of Arctic Sea Ice—Challenges and Strategies*, Polar Research Board, National Research Council, 92 pp., ISBN 978-0-309-26526-3, National Academies Press, Washington, D. C.

Nghiem, S. V. (2013), Arctic and Antarctic sea ice changes and impacts, Abstract C24A-01 presented at 2013 Fall Meeting, AGU, San Francisco, Calif., 9-13 Dec.

Nghiem, S. V., M. L. Van Woert, and G. Neumann (2005), Rapid formation of a sea ice barrier east of Svalbard, *J. Geophys. Res.*, *110*, C11013, doi:10.1029/2004JC002654.

Nghiem, S. V., P. Clemente-Colón, I. G. Rigor, D. K. Hall, and G. Neumann (2012), Seafloor control on sea ice, *Deep Sea Res. Part II*, *77–80*, 52–61, doi:10.1016/j.dsr2.2012.04.004.

Nghiem, S. V., et al. (2013), Studying Bromine, Ozone, and Mercury in the Arctic, *Eos, Trans. Amer. Geophys. Union*, *94*(33), 289–291.

National Snow and Ice Data Center (NSIDC) (2013), Bootstrap sea ice Concentrations from Nimbus-7 SMMR and DMSP SSM/I-SSMIS, Version 2. [Available at http://nsidc.org/data/nsidc-0079.html, accessed Nov. 2013.]

Ogi, M., and I. G. Rigor (2013), Trends in Arctic sea ice and the role of atmospheric circulation, *Atmos. Sci. Lett.*, *14*(2), 97–101, doi:10.1002/asl2.423.

Parkinson, C. L., and J. C. Comiso (2013), On the 2012 record low Arctic sea ice cover: Combined impact of preconditioning and an August storm, *Geophys. Res. Lett.*, *40*, 1356–1361, doi:10.1002/grl.50349.

Perovich, D. K., B. Light, H. Eicken, K. F. Jones, K. Ruciman, and S. V. Nghiem (2007), Increasing solar heating of the Arctic Ocean and adjacent seas, 1979-2005: Attribution and role in the ice-albedo feedback, *Geophys. Res. Lett.*, *34*, L19505, doi:10.1029/2007GL031480.

Perovich, D. K., J. A. Richter-Menge, K. F. Jones, B. Light, B. C. Elder, C. Polashenski, D. Laroche, T. Markus, and R. Lindsay (2011), Arctic sea-ice melt in 2008 and the role of solar heating, *Ann. Glaciol.*, *52*(57), 355-359, Part 2.

Perovich, D. K., W. Meier, M. Tschudi, S. Gerland, and J. Richter-Menge (2013), Sea ice cover, The Arctic, in State of the Climate in 2012, *Bull. Am. Meteorol. Soc.*, *94*(8), S126–S128.

Rawlins, M. A., M. Steele, M. C. Serreze, C. J. Vörösmarty, W. Ermold, R. B. Lammers, K. C. McDonald, T. M. Pavelsky, A. Shiklomanov, and J. Zhang (2009), Tracing freshwater anomalies through the air-land-ocean system: A case study from the Mackenzie River basin and the Beaufort Gyre, *Atmos. Ocean*, *47*(1), 79–97, doi:10.3137/OC301.2009.

Riggs, G. A., D. K. Hall, and V. V. Salomonson (2006), MODIS snow products user guide, 80 pp. [Available online at http://modis-snow-ice.gsfc.nasa.gov/uploads/sug_c5.pdf.]

Rigor, I. G. (2005), Interdecadal Variations in Arctic Sea Ice, PhD dissertation, 100 pp., Univ. of Washington, Seattle. [Available at http://www.atmos.washington.edu/academics/grads/PhDtheses/RigorI_PhD2005.pdf.]

Searcy, C., D. Kenneson, and W. Stringer (1996), A river-coast sea ice interaction model: Mackenzie River Delta, *J. Geophys. Res.*, *101*(C4), 8885–8894.

Shiklomanov, A. I., and R. B. Lammers (2011), River discharge, in *Arctic Report Card 2011*, pp. 156–161. [Available at http://www.arctic.noaa.gov/reportcard, accessed Jan. 2014.]

Simmonds, I., and I. Rudeva (2012), The great Arctic cyclone of August 2012, *Geophys. Res. Lett.*, *39*, L23709, doi:10.1029/2012GL054259.

Steffen, S., J. Bottenheim, A. Cole, T. A. Douglas, R. Ebinghaus, U. Friess, S. Netcheva, S. Nghiem, H. Sihler, and R. Staebler (2013), Atmospheric mercury over sea ice during the OASIS-2009 campaign, *Atmos. Chem. Phys.*, *13*, 7007–7021, doi:10.5194/acp-13-7007-2013.

Turner, J. K., and J. R. Gyakum (2010), Trends in Canadian surface temperature variability in the context of climate change, *Atmos. Ocean*, *48*(3), 147–162, doi:10.3137/AO1102.2010.

Woo, M. K., and R. Thorne (2003), Streamflow in the Mackenzie Basin, Canada, *Arctic*, *56*(4), 328–340.

Zhang, J. L., R. Lindsay, A. Schweiger, and M. Steele (2013), The impact of an intense summer cyclone on 2012 Arctic sea ice retreat, *Geophys. Res. Lett.*, *40*, 720–726, doi:10.1002/grl.50190.

Effects of Mackenzie River discharge and bathymetry on sea ice in the Beaufort Sea

S. V. Nghiem[1], D. K. Hall[2], I. G. Rigor[3], P. Li[1], and G. Neumann[1]
[1]Jet Propulsion Laboratory, California Institute of Technology, Pasadena, California, USA
[2]NASA Goddard Space Flight Center, Greenbelt, Maryland, USA
[3]University of Washington, Seattle, Washington, USA

Introduction

The auxiliary material includes: two tables and five figures. The first table (Table S1) is for the shortest distances and steepest slopes between the 25-m isobath to the 10-m isobath and to the 50-m isobath from IBCAO Version 3. The second table (Table S2) contains information of Arctic rivers. The first figure (Figure S1) shows the conformance of sea ice patterns to bathymetry. The second figure (Figure S2) shows fingers of open water from Mackenzie warm waters intruded into the band of landfast sea ice observed by MODIS. The third and fourth figures (Figures S3 and S4) are for surface temperature of open water in the Beaufort Sea. The last figure (Figure S5) presents the watershed of Mackenzie River.

1. Table S1: Shortest distances and steepest slopes between the 25-m isobath to the 10-m isobath and to the 50-m isobath from IBCAO Version 3. The shortest distance is calculated as the radius of the smallest circle with its center located on the 25-m isobath and its perimeter touched the 10-m (or 50-m) isobath. The steepest slope is the ratio of the depth change between 25 m and 10 m (or 50 m) over the respective shortest distance. In all cases, the edge of landfast ice (6/14/2012) and the lead in 2013 (5/17/2013) were closely located along the 25-m isobath. This result illustrates that sea ice patterns conform to bathymetric depth and do not depend on bathymetric slope.

1.1 Column “Longitude on 25-m isobath”, degrees, west longitude on the 25-m isobath.

1.2 Column “Distance between 25-m and 10-m isobath”, km.

1.3 Column “Slope between 25-m and 10-m isobath”, m/km.

1.4 Column “Distance between 25-m and 50-m isobath”, km.

1.5 Column “Slope between 25-m and 50-m isobath”, m/km.

2. Table S2: Watersheds of several large rivers in the Arctic. Data from ArcticRIMS, a Regional, Integrated Hydrological Monitoring System for the Pan-Arctic Land Mass, available on the Internet at http://rims.unh.edu/, accessed Dec. 2013. For comparison, the total surface area of Greenland is 2,166,086 km^2.

2.1 Column “River”, river name.

2.2 Column “Watershed”, km^2, area of watershed.

2.3 Column :Southernmost reach", degree, north latitude of the watershed southernmost reach.

2.4 Column "Sea basin", name, the sea to which the river discharge goes.

3. Figure S1: Edge of the landfast sea ice on 14 June 2012 (white curve) and edge of the lead on 17 May 2013 (yellow curve), observed with MODIS satellite data, overlain on the IBCAO bathymetry map from Version 2 (panel a) and Version 3 (panel b). The ice edges conform well to the 25-m isobath except over the local seafloor features marked inside the red ellipse. Those features were erroneous artifacts in IBCAO Version 2, and were corrected by new survey data in IBCAO Version 3. Sea ice patterns are thus affected by depth and independent of seafloor slope.

4. Figure S2: Fingers of open water (dark blue) from Mackenzie warm waters intruded into the band of landfast sea ice (light blue) observed by MODIS on 14 June 2012, when the river discharge had not yet broken through the landfast ice barrier spanning across the Mackenzie Delta.

5. Figure S3: Open-water surface temperature (OWST) in ^{o}C: Panel a for 5 July 1998, and panel b for 5 July 2008 (same day and month as in Figure 3 for 2012) overlain on IBCAO Version 3 bathymetry. These results are from the Pathfinder, Level 3, Version 5, Advanced Very High Resolution Radiometer (AVHRR) sea surface temperature product at ftp://podaac-ftp.jpl.nasa.gov/OceanTemperature/avhrr/L3/pathfinder_v5/ (accessed Dec., 2013). OWST data are not valid in cloud-covered or sea ice areas, which appear as missing data in the maps.

6. Figure S4: Open-water surface temperature (OWST) in ^{o}C, measured by MODIS AG1 on 5 July 2008 (same day and month as in Figure 3 for 2012). This is similar to the AVHRR OWST map on the same date (auxiliary Figure S3b); however, the difference between MODIS and AVHRR cloud and ice masking results in some differences in missing data areas. For 5 July 1998, MODIS had not been launched yet and thus MODIS data were not available to obtain the 1998 OWST map. See auxiliary Figure S3a for OWST map from AVHRR on 5 July 1998.

7. Figure S5: Mackenzie River watershed, represented by the blue region in North America, with a basin area of 1.8 million km^2 reaching south to 53^{o}N. This map is adapted from North America Watersheds, Cooperative Educational Service Agency 10 (CESA 10), available on the Internet at http://moodle.cesa10.k12.wi.us/, accessed Nov. 2013.

Table S1. Shortest distances and steepest slopes between the 25-m isobath to the 10-m isobath and to the 50-m isobath from IBCAO Version 3. The shortest distance is calculated as the radius of the smallest circle with its center located on the 25-m isobath and its perimeter touched the 10-m (or 50-m) isobath. The steepest slope is the ratio of the depth change between 25 m and 10 m (or 50 m) over the respective shortest distance. In all cases, the edge of landfast ice (6/14/2012) and the lead in 2013 (5/17/2013) were closely located along the 25-m isobath. This result illustrates that sea ice patterns conform to bathymetric depth and do not depend on bathymetric slope.

Longitude on 25-m isobath	Distance between 25-m and 10-m isobath	Slope between 25-m and 10-m isobath	Distance between 25-m and 50-m isobath	Slope between 25-m and 50-m isobath
137.16°W	6.5 km	2.31 m/km	14.8 km	1.69 m/km
136.81°W	19.3 km	0.78 m/km	15.9 km	1.57 m/km
134.70°W	22.3 km	0.67 m/km	29.3 km	0.85 m/km
132.23°W	18.7 km	0.80 m/km	51.4 km	0.49 m/km
131.37°W	16.1 km	0.93 m/km	54.7 km	0.46 m/km
129.38°W	34.8 km	0.43 m/km	40.7 km	0.61 m/km

Table S2. Watersheds of several large rivers in the Arctic. Data from ArcticRIMS, a Regional, Integrated Hydrological Monitoring System for the Pan-Arctic Land Mass, available on the Internet at http://rims.unh.edu/, accessed Dec. 2013. For comparison, the total surface area of Greenland is 2,166,086 km^2.

River	Watershed	Southernmost reach	Sea basin
Mackenzie	1,783,912 km^2	52.2°N	Beaufort Sea
Yukon	833,232 km^2	58.8°N	Bering Strait
Ob	2,994,238 km^2	45.3°N	Kara Sea
Yenisei	2,537,404 km^2	45.7°N	Kara Sea
Lena	2,460,742 km^2	52.2°N	Laptev Sea
Kolyma	651,631 km^2	60.6°N	East Siberian Sea

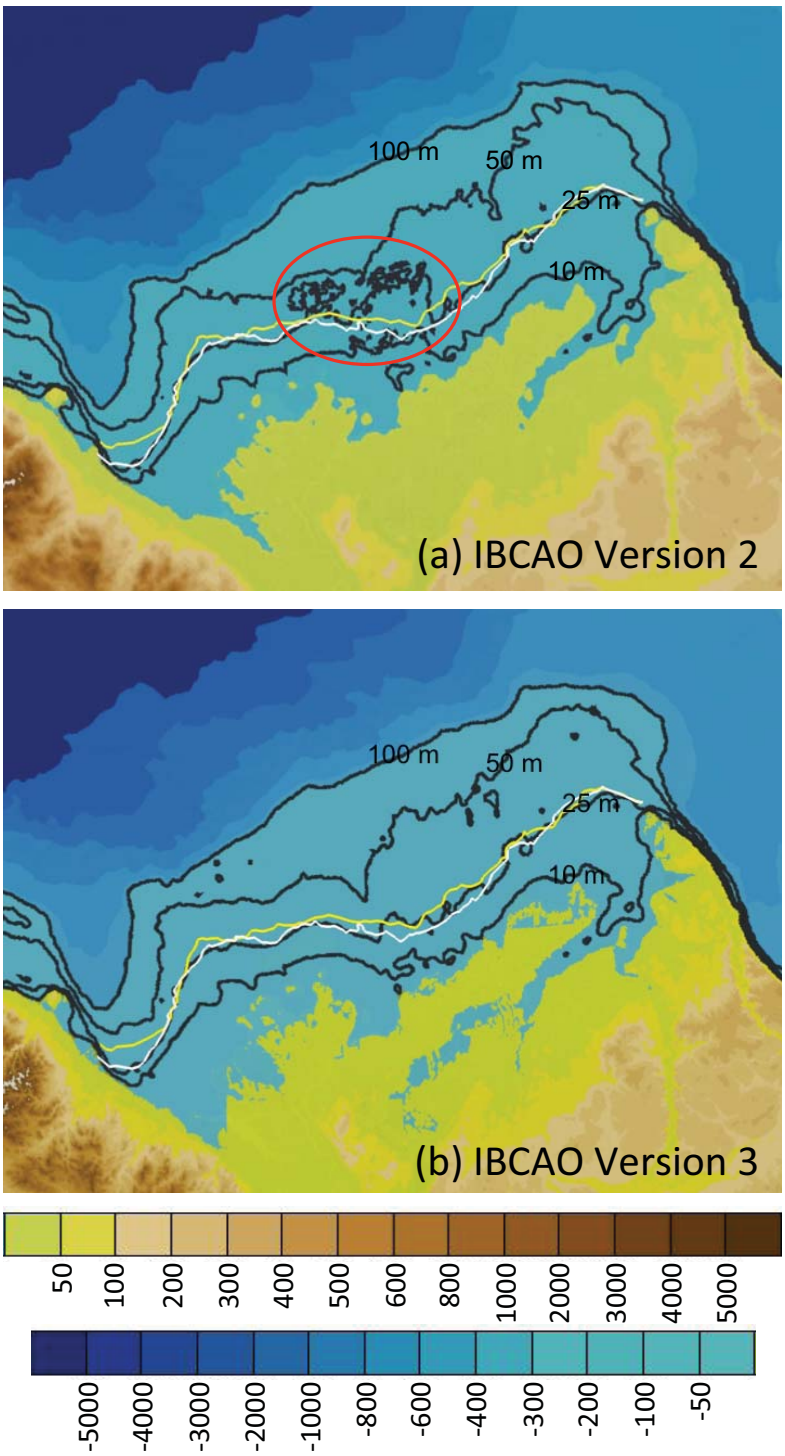

Figure S1. Edge of the landfast sea ice on 14 June 2012 (white curve) and edge of the lead on 17 May 2013 (yellow curve), observed with MODIS satellite data, overlain on the IBCAO bathymetry map from Version 2 (panel a) and Version 3 (panel b). The ice edges conform well to the 25-m isobath except over the local seafloor features marked inside the red ellipse. Those features were erroneous artifacts in IBCAO Version 2, and were corrected by new survey data in IBCAO Version 3. Sea ice patterns are thus affected by depth and independent of seafloor slope.

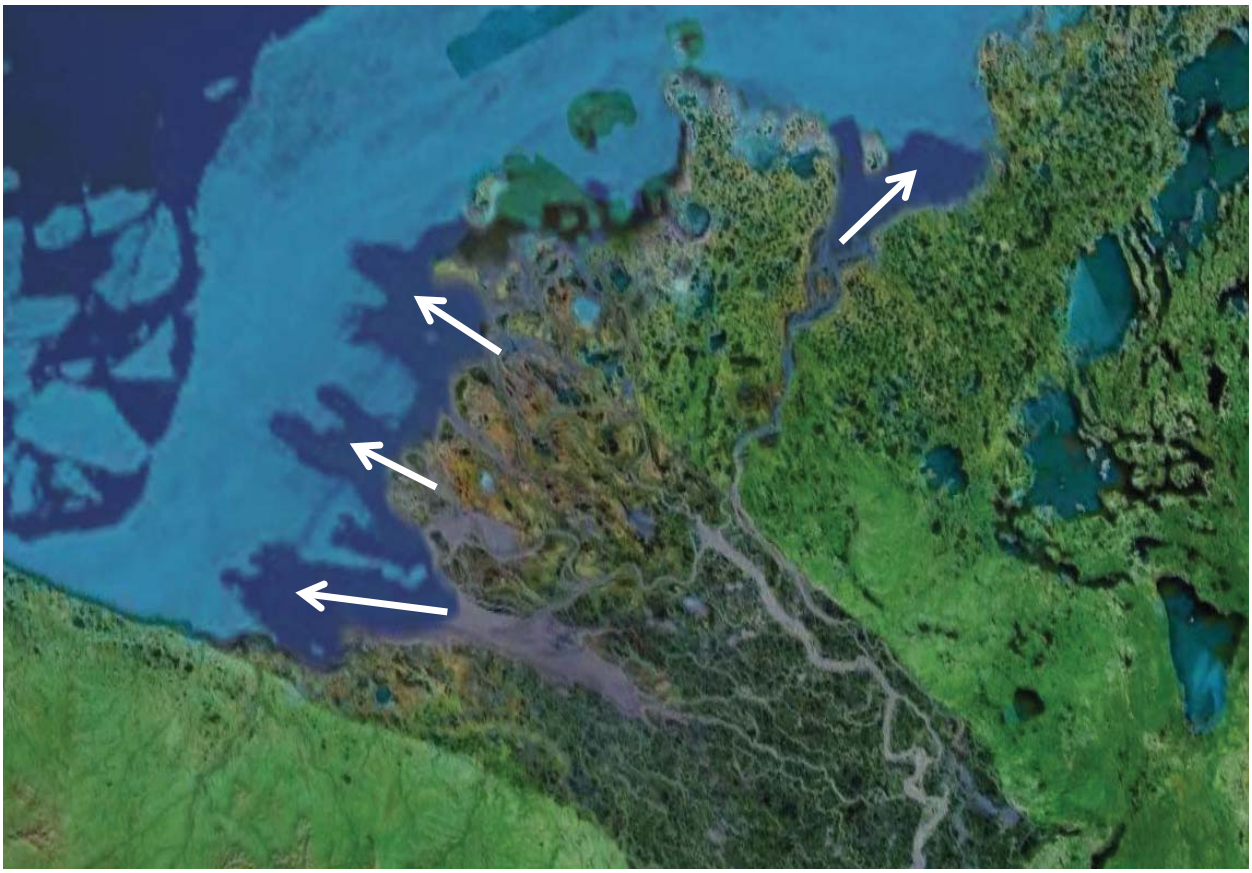

Figure S2. Fingers of open water (dark blue) from Mackenzie warm waters intruded into the band of landfast sea ice (light blue) observed by MODIS on 14 June 2012, when the river discharge had not yet broken through the landfast ice barrier spanning across the Mackenzie Delta.

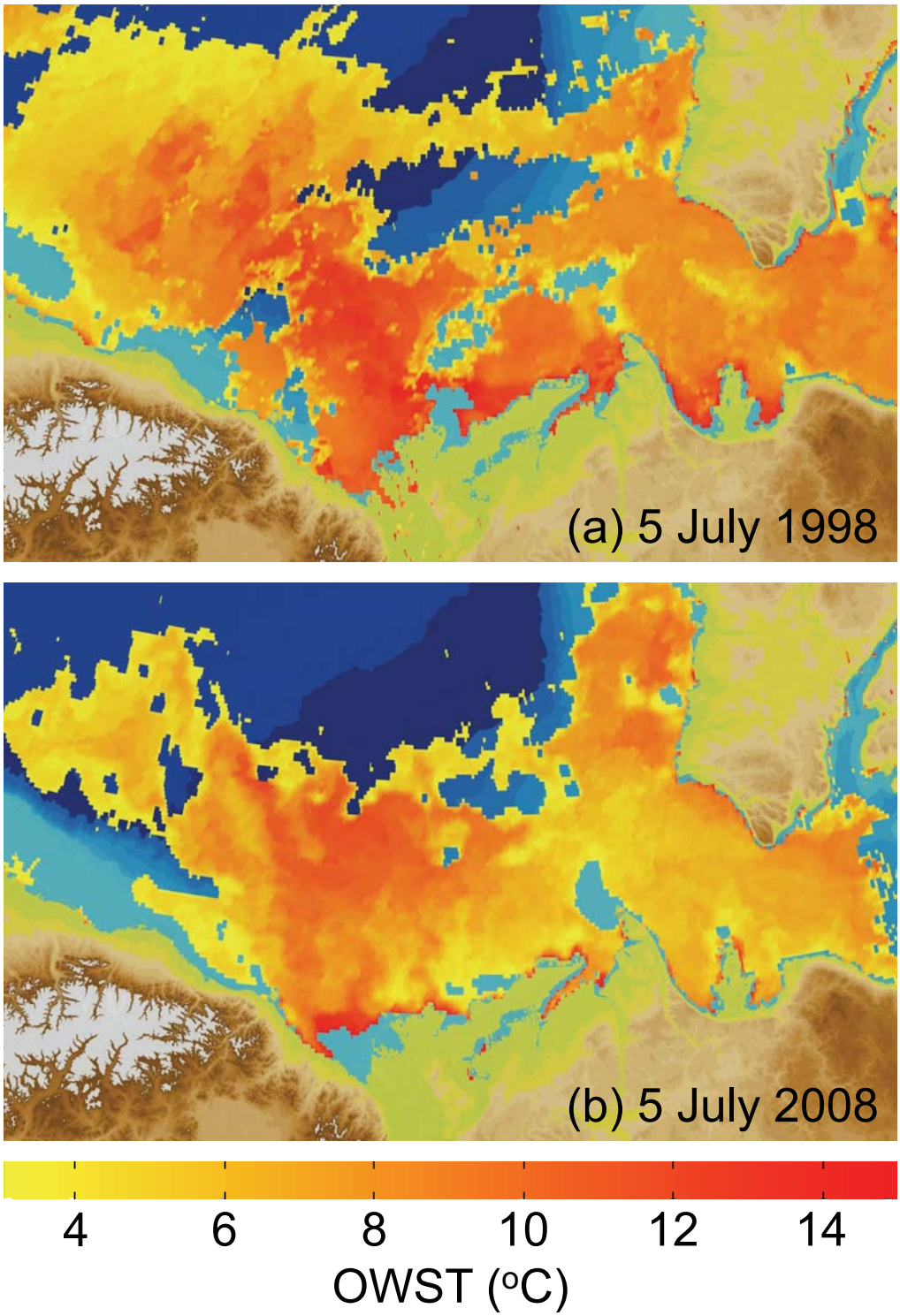

Figure S3. Open-water surface temperature (OWST) in oC: Panel a for 5 July 1998, and panel b for 5 July 2008 (same day and month as in Figure 3 for 2012) overlain on IBCAO Version 3 bathymetry. These results are from the Pathfinder, Level 3, Version 5, Advanced Very High Resolution Radiometer (AVHRR) sea surface temperature product at ftp://podaac-ftp.jpl.nasa.gov/OceanTemperature/avhrr/L3/pathfinder_v5/ (accessed Dec., 2013). OWST data are not valid in cloud-covered or sea ice areas, which appear as missing data in the maps.

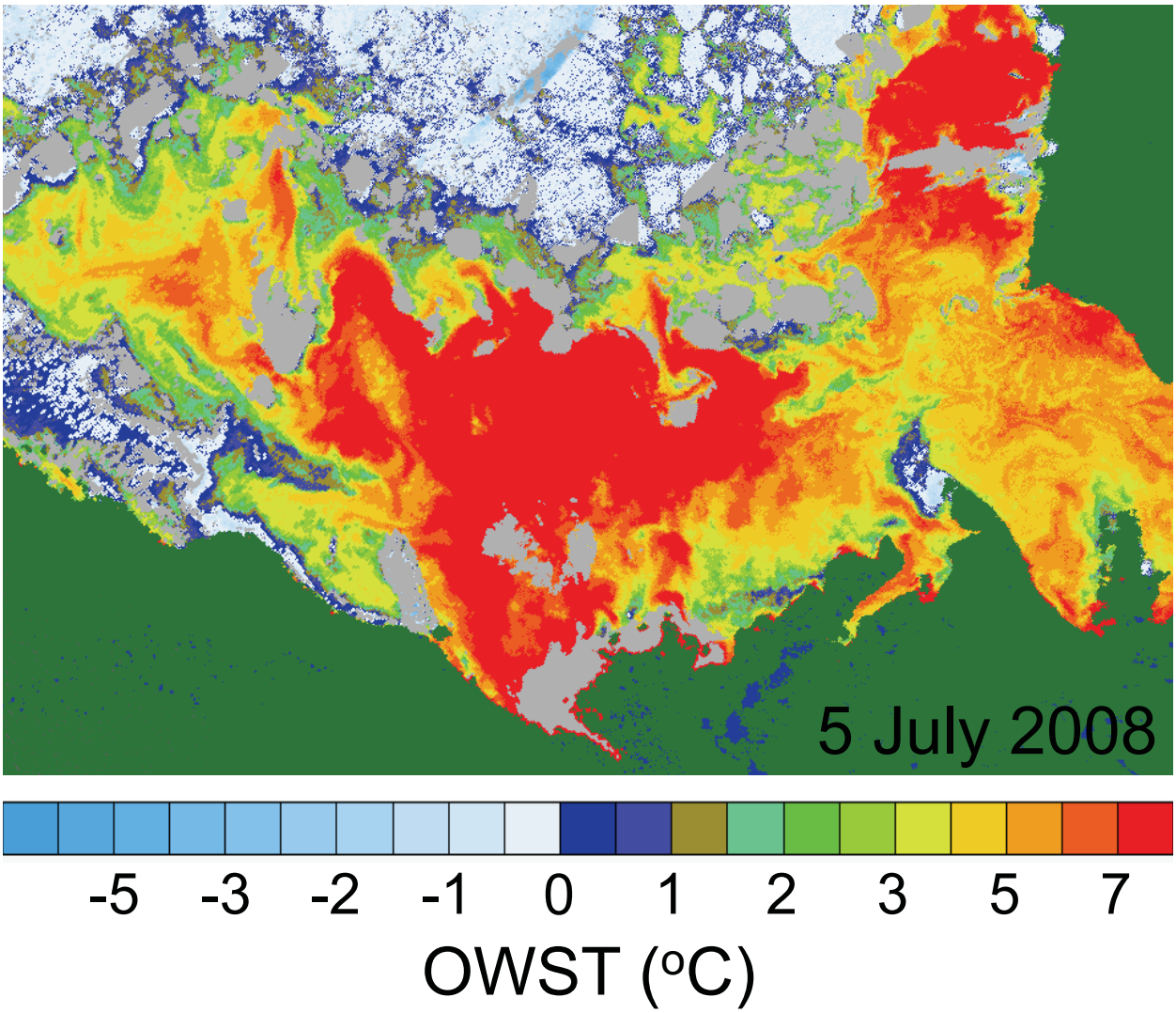

Figure S4. Open-water surface temperature (OWST) in oC, measured by MODIS AG1 on 5 July 2008 (same day and month as in Figure 3 for 2012). This is similar to the AVHRR OWST map on the same date (auxiliary Figure S3b); however, the difference between MODIS and AVHRR cloud and ice masking results in some differences in missing data areas. For 5 July 1998, MODIS had not been launched yet and thus MODIS data were not available to obtain the 1998 OWST map. See auxiliary Figure S3a for OWST map from AVHRR on 5 July 1998.

Figure S5. Mackenzie River watershed, represented by the blue region in North America, with a basin area of 1.8 million km2 reaching south to 53oN. This map is adapted from North America Watersheds, Cooperative Educational Service Agency 10 (CESA 10), available on the Internet at http://moodle.cesa10.k12.wi.us/, accessed Nov. 2013.